Volume 17, Number 1, 2024. pp. 75-85

Jordan Journal of Physics

ARTICLE

Secondary Phases, Morphology and Band Tails of Third Generation Photovoltaic Absorber Layer CZTS Annealed at Different Temperatures

Adnan H. Mini[a], **Mohammad B. Karaman**[b], **Muhammed A. Batal**[b] and **Ahmed K. Kbetri**[b]

[a] *Department of Physics, College of Science, Tishreen University, Latakia, Syria.*
[b] *Department of Physics, College of Science, Aleppo University, Aleppo, Syria.*

Doi: **https://doi.org/10.47011/17.1.7**

Received on: 10/05/2022; *Accepted on: 04/07/2022*

Abstract: In this work, we have successfully fabricated Cu_2ZnSnS_4 (CZTS) thin films using the sol-gel spin-coating technique. Thin films were annealed in an argon atmosphere at different temperatures of 350, 375, 400, 425, and 450 °C for an hour. The influence of annealing temperature on structural, morphological, and optical properties was investigated. x-ray diffraction measurement confirmed the formation of secondary phases in as-deposited and annealed thin films at 350 and 375 °C. A pure kesterite phase was obtained at an annealing temperature of 400 °C, but degradation occurred at higher temperatures. The morphology study of the surface structure showed that thin films have homogeneous surfaces. The Volmer-Weber mode was the dominating growth mode. The as-deposited and annealed CZTS thin films exhibited a high absorption coefficient of the order of 10^4 cm^{-1}, and the optical energy band gap E_g was red-shifted with increasing annealing temperature. The optical study showed a decrease in Urbach tail energy with an increase in annealing temperature and reached 0.39 eV at 400 °C. The refractive index and dielectric constants of CZTS thin films were calculated.

Keywords: Cu_2ZnSnS_4 thin films, Sol-Gel technique, Secondary phases, Roughness parameters, Band gap, Urbach tails.

Introduction

Electric power production from renewable energy sources has now become an important replacement for the generation of electric power from limited carbon-based fossil energy. Solar energy is one of the most cost-effective and sustainable energy resources. Photovoltaic technology provides direct and effective conversion of solar energy into electrical energy [1]. Recently, $Cu(In,Ga)(S,Se)_2$ thin-film photovoltaic cells showed high energy conversion with an efficiency of more than 20%. These cells could be used as viable alternatives to silicon-based photovoltaic cells [2]. However, the presence of some rare and expensive elements in their synthesis, such as indium and gallium, can limit the large-scale production of these cells [3]. Emerging copper zinc tin sulphide (CZTS)-based kesterite photovoltaic cells have attracted the observation of researchers due to the abundance of their materials, low cost, and non-toxicity. The thin-film semiconductor of CZTS plays a key role in absorbing sunlight and converting it into electricity. Such types of films have structural, optical, and electrical properties that profoundly affect the overall performance of the photovoltaic cell.

Corresponding Author: Ahmed Khaled Kbetri **Email**: ahmed.kbetri@tishreen.edu.sy

The CZTS thin film has a quaternary crystalline kesterite structure similar to that of $Cu(In,Ga)(S,Se)_2$ [4]. Its p-type electrical conductivity is suitable for serving as the absorptive layer of photovoltaic cells [2]. CZTS does not contain scarce or harmful elements and shares similar properties with $Cu(In, Ga)(S, Se)_2$, making it an appropriate alternative. Kesterite exhibits highly favorable optical properties for photovoltaic applications, including a direct band gap ranging from 1.4 to 1.6 eV [5], which is very close to the optimum value of the absorbent layer in photovoltaic cells. Moreover, kesterite has a high absorption coefficient of about 10^4 cm^{-1} in the visible light region [6]. However, despite these unique characteristics, the four-element composition of kesterite increases the potential for the formation of secondary, such as CuS, ZnS, Cu_2S, SnS_{2-x}, and ternary, such as Cu_2SnS_3, phases during the deposition process [7]. The secondary phases cause localized states to extend in the band gap, thus affecting its value. They can also cause an impediment to the mobility of charge carriers [8]. It is strongly desirable to completely remove or at least avoid the formation of secondary phases during the preparation process. Post-annealing is one of the most important ways to remove such phases and improve the crystallization of deposited films. Kumar and Ingole [9] studied the effect of annealing with the sulfur atmosphere on the various physical properties of CZTS thin films prepared by the sol-gel method applying the spin-coating technique. They found that treatment at 530 °C for 30 min is optimal. In the same context, Ziti *et al.* [10] also studied the effect of annealing treatment with an atmosphere of H_2S gas on the optical properties of thin films of CZTS, with an energy band gap of 1.56 eV. Despite the suitability of these films for photovoltaic applications, it's important to highlight that the annealing conditions involve the use of toxic and hazardous gases.

In this paper, CZTS thin films were prepared by sol-gel spin-coating technique and annealed in a safe atmosphere of argon gas at temperatures of 350, 375, 400, 425, and 450 °C for one hour. The impact of annealing in an argon atmosphere on the films' structural, morphological, and optical properties was studied.

Experimental Details

Materials

Zinc acetate ($(CH_3COO)_2.Zn.2H_2O$ 99.9%), copper chloride ($CuCl_2$ 98%), tin tetrahydrochloride ($SnCl_4.5H_2O$ 98%), thiourea (H_2NCSNH_2 99.9%), 2-Metoxyethanol ($HOCH_2CH_2OCH_3$ 99.5%), and monoethanolamine (C_2H_7NO 99.5%) were used for production of CZTS sol-gel solution. All chemicals used in the present investigation were analytical grade.

Method of Preparing CZTS Thin Film

The CZTS thin film preparation process is divided into four stages: precursor solution preparation, substrate preparation, deposition of thin films on the substrate, and annealing treatment.

Precursor Solution Preparation

The solution was prepared with a stoichiometric ratio of the reactants Cu:Zn:Sn:S aiming for a concentration of 0.1 mol/L. Initially, 0.2 mol of $CuCl_2$ and 0.1 mol of $SnCl_4.5H_2O$ were dissolved in 100 mL of 2-methoxyethanol solution at laboratory temperature using a magnetic stirrer until a bluish-green solution was obtained. Then, 0.1 mol of $(CH_3COO)_2.Zn.2H_2O$ was added while stirring the solution. As the $(CH_3COO)_2.Zn.2H_2O$ dissolved, the color of the solution turned a greenish-yellow, indicating that zinc acetate facilitated the oxidation and reduction reaction between copper ions $2Cu^{+2}$ and tin ions Sn^{+2} leading to the formation of $2Cu^{+}$ and Sn^{+4} [11]. Finally, the temperature of the solution was gradually raised. When it reached 45 °C, 0.4 mol of thiourea was added. An extra amount of thiourea was added to the solution to neutralize the loss of sulfur during the drying of the thin film [12]. After that, 0.5 mL of monoethanolamine was added as a stabilizer, causing the solution to become a weak transparent color. After the solution was left on the magnetic stirrer for two hours, the color of the solution changed to a pure light yellow, indicating the formation of the CZTS solution. Fig. 1(a) shows the evolution of the precursor solution preparation process.

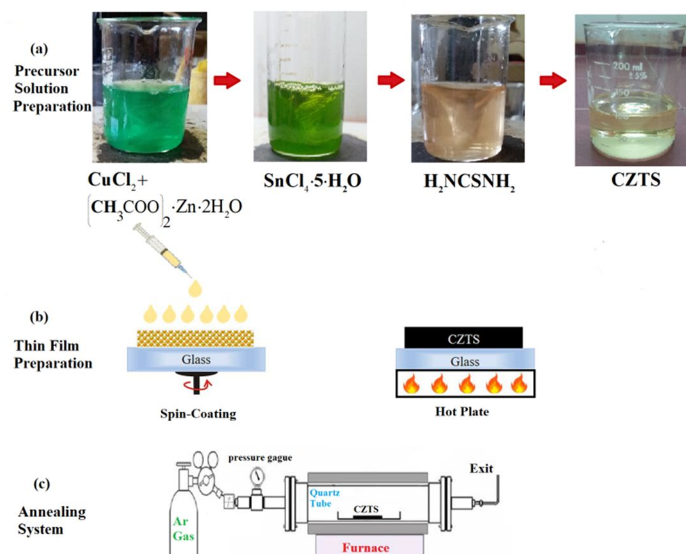

FIG. 1. CZTS thin film preparation scheme, (a) precursor solution, (b) thin film depositing, (c) annealing system.

Substrate Preparation

Soda-lime glass substrates were cleaned by an alkaline solution method before starting the deposition process. Firstly, the substrates were placed in a solution of sodium hydroxide dissolved in distilled water, with a concentration of 1 mol/L, for 5 minutes. Then the substrates were transferred to a solution of hydrochloric acid, also with a concentration of 1 mol/L, for another 5 minutes, to neutralize the alkaline attack on the glass surface. After that, the substrates were put in distilled water for 20 minutes. Finally, the substrates were dried and become ready for the deposition process.

Thin Films Preparation

Semiconductor thin films of CZTS were deposited on a glass substrate by the sol-gel spin-coating technique. A homemade spin-coater device was used for depositing thin films with a rotation speed of up to 7000 rpm. The prepared solution was spin-coated on the substrate at a rotation speed of 3000 rpm for 30 s. The substrate was then dried directly on a hot plate at a temperature of 250 °C for 5 min to remove the organic solvent. Thus, we obtained a thin film with a thickness of one layer. The process was repeated until we obtained a thin film with a thickness of ten layers. Finally, we have prepared a semiconductor thin film from CZTS. Fig. 1(b) shows the preparation process of the thin film.

Annealing of Thin Films CZTS

CZTS thin films were annealed in an argon atmosphere using a quartz tube furnace. The atmosphere of the tube was purged with argon gas for 30 min before starting the annealing process. Fig. 1(c) shows the designed annealing system. CZTS thin films were annealed in an argon atmosphere at 350, 375, 400, 425, and 450 °C for one hour.

Characterization

The crystal structure and the formed phases were studied using a Leybold Didactic x-ray diffraction device equipped with a copper anode that emits x-rays with a wavelength of $\lambda = 0.154$ nm in the 2θ range of 20°-70°. The morphological characteristics were studied using an atomic force microscope AFM Naio-type. The optical properties were studied using a spectrophotometer (UV-VIS-NIR) type JASCO V670.

Results and Discussion

Structural Measurements

X-RAY Diffraction Measurements

The structures of as-deposited and annealed thin films were studied using an x-ray diffraction device, and the x-ray diffraction spectra were processed and analyzed using X'Pert HighScore Plus software. Fig. 2(a) illustrates the x-ray diffraction spectra of as-deposited and annealed thin films. In Fig. 2(b), JCPDS reference cards used to analyze these spectra are shown.

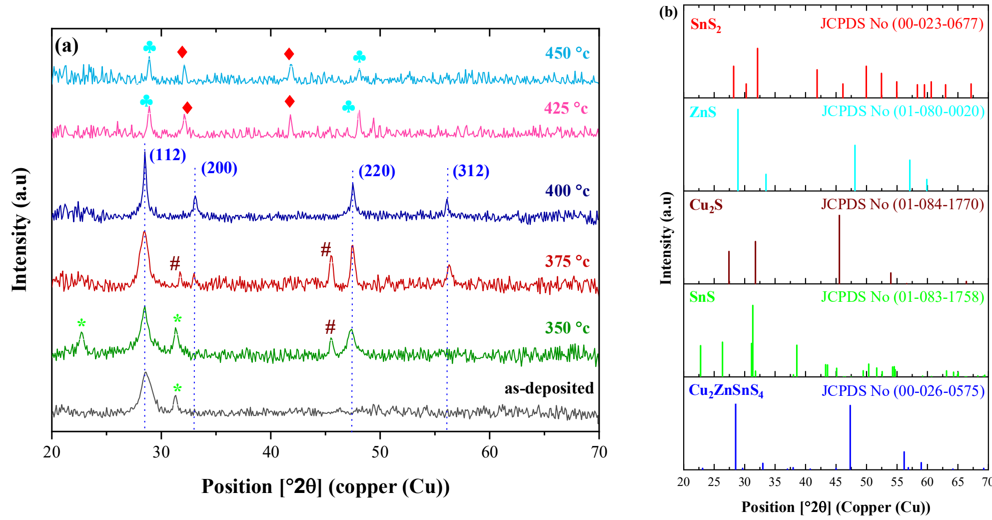

FIG. 2. (a) XRD pattern of CZTS thin films, (b) JCPDS reference cards used in the x-ray diffraction spectral analysis.

As shown in Fig. 2(a), the as-deposited film showed a poor crystalline structure in agreement with previous studies [13]. The annealing of up to 400 °C results in the formation of a pure polycrystalline kesterite structure, consistent with previous works [14, 15]. Fig. 2(a) shows the appearance of peaks at positions 2θ = 28.5º, 2θ = 32.9º, 2θ = 47.3º, and 2θ = 56.3º for crystal orientation plans (112), (200), (220), and (312), respectively. These planes belong to the CZTS kesterite structure according to the JCPDS reference card No.(00-026-0575) for thin films annealed at 400 °C.

Fig. 2(a) illustrates that peaks of secondary phases indicated by (*) and (#) correspond to the SnS and Cu_2S phases, respectively, according to their JCPDS reference cards No.(01-083-1758) and No.(01-084-1770). This observation is consistent with previous studies [7, 16]. However, upon raising the annealing temperature to 425 and 450 °C, a decomposition of the kesterite phase was observed with the appearance of the secondary phase of ZnS referred to by symbol (♣), according to the JCPDS reference card No.(01-080-0020). Moreover, the secondary phase of SnS_2 is referred to by the symbol (♦), according to the JCPDS reference card No.(00-023-0677), appeared.

The $d_{hk\ell}$ distance between the (112) crystal planes of the preferred orientation of kesterite was calculated using the following Bragg formula [17]:

$$2d_{hk\ell} \cdot sin\theta_{hk\ell} = m\lambda \tag{1}$$

where $d_{hk\ell}$ is the distance between parallel crystal planes according to direction $(hk\ell)$, $\theta_{hk\ell}$ is Bragg diffraction angle, and m is the diffraction order.

The $d_{hk\ell}$ was found to be equal to 3.153Å, 3.142Å, 3.142Å, and 3.131Å for the as-deposited film, and annealed at 350, 375, and 400 °C, respectively. These values are in excellent agreement with Ref. [18].

The crystallite size D was calculated for as-deposited and annealed thin films at the (112) crystal orientation plane using the Debye-Scherrer formula [19]:

$$D = \frac{k\lambda}{\beta cos\theta_{hk\ell}} \tag{2}$$

where k is a dimensionless constant that takes the value $k = 2[ln(2)/\pi]^{1/2} = 0.939$ [19] and β is the full width at half maximum (FWHM) intensity of the diffraction peak measured in radians.

The strain ε in the crystal lattice is defined as a slight displacement of the atoms relative to their natural lattice positions, imposed by crystal defects, such as dislocations and impurities. ε was calculated using the following equation [20]:

$$\varepsilon = \frac{\beta cos\theta_{hk\ell}}{4}. \tag{3}$$

The dislocation density δ, which is defined as the length of the dislocation lines per unit crystal size, can be obtained using crystallite size D by [20]:

$$\delta = \frac{1}{D^2} \tag{4}$$

Table 1 shows the calculated values of the crystallite size D, the strain in the crystal lattice ε, and the dislocation density δ.

TABLE 1. Values of crystallite size D, lattice strain ε, and dislocation density δ of the CZTS thin films.

Thin Film	$2\theta(\deg)$	FWHM $\beta(\deg)$	crystallite size $D(nm)$	lattice strain $(\times10^{-3})$ (ε)	dislocation density (δ) $(\times10^{16} Lin.m^{-2})$
As-deposited	28.3	1.8	4.755	7.612	4.423
350 °C	28.4	1.4	6.113	5.921	0.027
375 °C	28.4	1.3	6.583	5.498	0.023
400 °C	28.5	0.3	28.528	1.269	0.001

The strain in the crystal lattice decreases with the increase in the annealing temperature in CZTS thin films, as illustrated in Table 1. Increasing the annealing temperature leads to a decrease in FWHM and consequently to an increase in crystallite size D, which is in agreement with [21]. This behavior reduces defects at the crystalline boundaries that appear when the crystallite size is small [22]. According to the Williamson-Hall uniform-anisotropic deformation energy-density model, the surface tension of very small grains increases the internal pressure of the grain and thus creates an internal pressure field. The pressure at the crystal boundary causes an increase in the strain in the crystal lattice [23]. The intensity of dislocations also decreased with the increase in the annealing temperature. This indicates an enhancement in the purity of the kesterite phase by increasing the annealing temperature up to 400 °C.

Lattice constants a = b and c of the tetragonal system of kesterite CZTS can be calculated using the relation [17]:

$$\frac{1}{d_{hk\ell}^2} = \frac{4sin^2(\theta_{hk\ell})}{\lambda^2} = \frac{h^2+k^2}{a^2} + \frac{\ell^2}{c^2} \quad (5)$$

where h, k, and ℓ on the right-hand side are Miller's indices.

The value of lattice constants, the ratio c/2a, and the cell volume V for CZTS thin films are introduced in Table 2.

TABLE 2. Values of lattice constants a = b, c, $c/2a$ ratio, and primary cell volume V for as-deposited and annealed CZTS thin films at different temperatures.

Thin Film	$(h\,k\,\ell)$	d (Å)	a = b (Å)	c (Å)	c/2a	$V(Å)^3$
As-deposited	(112) -	3.153 -	-	-	-	-
350 °C	(112) (220)	3.142 1.928	5.435	10.917	1.005	322.480
375 °C	(112) (220)	3.142 1.928	5.435	10.917	1.005	322.480
400 °C	(112) (220)	3.132 1.918	5.425	10.848	1	319.263
JCPDS No.(00-026-0575)	(112) (220)	3.126 1.919	5.427	10.848	1	319.263

Table 2 shows the decreasing value of the lattice constant c when the annealing temperature reaches 400 °C. This may be due to the decomposition of the impurity phases, which led to an ideal value of 1 and thus formed a pure quaternary phase of kesterite [24].

Morphological Study

The morphology of thin films is one of the most significant properties in understanding surface phenomena. AFM was used to study the surface morphologies of the as-deposited and annealed CZTS thin films to decide how the annealing temperature affected the surface morphology of thin films. The size of the scanned area was (12.1 μm × 12.1 μm). We acquired 2D and 3D images of the CZTS thin film surfaces using the Nanosurf software connected with the AFM device. These images were analyzed using Mountain's lab software. Fig. 3 shows 2D and 3D images of CZTS thin films.

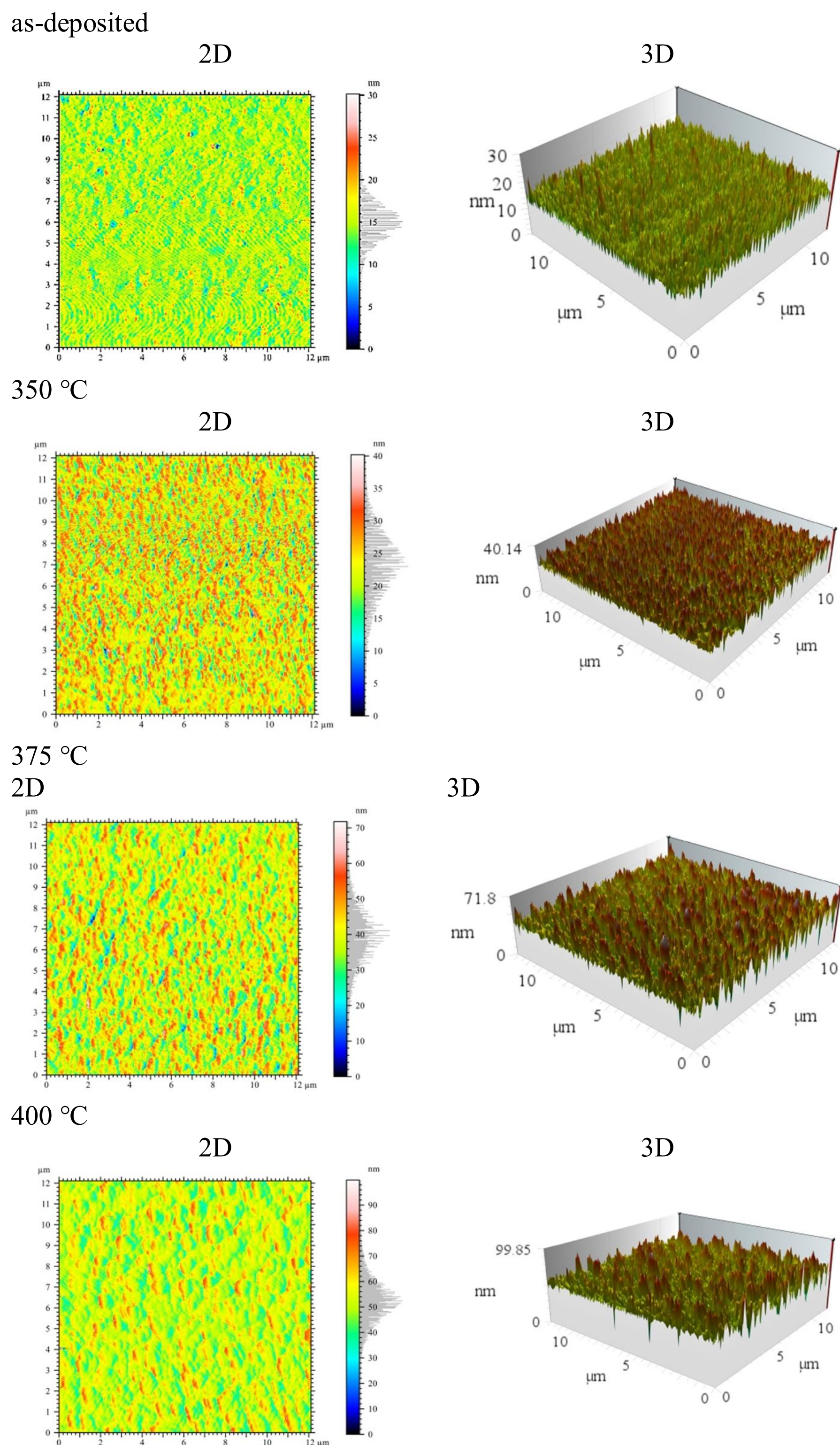

FIG. 3. 2D and 3D images of CZTS thin films annealed at different temperatures.

The AFM images revealed that the thin films have a homogeneous surface topography where the dominant grain growth mode is the Volmer–Weber mode [25].

The roughness parameters were estimated according to ISO 25178 using Mountain's lab software, as organized in Table 3.

TABLE 3. Roughness parameters according to ISO 25178 Roughness ISO 25178.

Height parameters	as-deposited	350 °C	375 °C	400 °C
Root mean square heights (RMS) (nm)	1.26	2.575	7.719	7.971
Skewness of the height distribution (S_{sk})	0.1434	-0.3799	-0.128	0.2094
Kurtosis of the height Distribution (S_{ku})	3.244	3.885	3.478	3.573
Maximum peak height (S_z) (nm)	15.30	24.95	71.80	99.85
Density of peaks (S_{pd}) ($\frac{1}{\mu m^2}$)	23.25	19.10	5.779	3.394
Arithmetic means peak curvature (S_{pc})	2.011	3.461	4.529	4.966

Table 3 shows the increase in the root-mean-square heights (surface roughness) of the CZTS films with the increase in the annealing temperature. This can be explained by the enlargement of the grain size due to the improvement of the growth during the annealing process. It is observed from Fig. 3 that the average size of the grain gets larger with the increase in annealing temperature. This can be attributed to the increase in annealing temperature, which enhances surface mobility. Thus, the merging of the grains with each other, forming larger grains, decreases the density of the number of peaks per unit area S_{pd}. The S_{pd} reached its lowest value and was equal to 3.394 $\frac{1}{\mu m^2}$ for the film annealed at 400 °C. The images in Fig. 3 show the presence of deep depressions in the surface of the annealed films at 350 and 375 °C indicated by the negative value of the skewness S_{sk} shown in Table 3. S_{sk} determines the asymmetry of the height distribution. All thin film grains showed sharp peaks confirmed by the large value of the kurtosis of the height distribution S_{ku}, which qualifies the flatness of the height distribution. The grains tend to be rounded in the thin film annealed at 400°C as shown by the large value of the arithmetic mean peak curvature S_{pc}, which is defined as the arithmetic mean of the principal curvatures of peaks. S_{pc} is enabled to know the mean form of the peaks: either pointed or rounded, according to the mean value of the curvature of the surface at these points; the higher the value, the more rounded the peaks.

The films treated at 425 and 450°C were excluded from the study due to the decomposition of the kesterite phase at these degrees in the x-ray diffraction spectra.

Optical Properties

Transmittance Spectrum and Absorption Coefficient of CZTS Thin Films

The optical properties of the as-deposited and annealed CZTS films at different temperatures were studied using a JASCO spectrophotometer within the range of 300-1500 nm. In Fig. 4(a), the transmittance spectra of CZTS thin films are shown. It can be seen that the transmittance of CZTS thin films is minimal in the visible region. The value of the absorbent material has to be very high for photovoltaic thin-film applications [26]. The absorption coefficient α of as-deposited and annealed CZTS films was determined from the transmittance spectrum, as given by the relationship [27]:

$$\alpha = \frac{1}{d}\ln\left(\frac{1}{T}\right) \quad (6)$$

where d and T are the thickness and transmittance of the thin film, respectively.

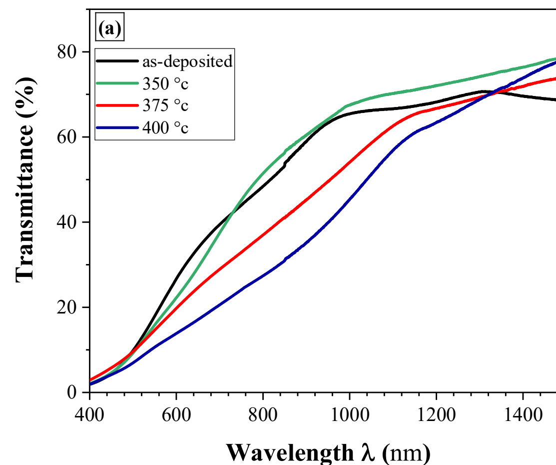

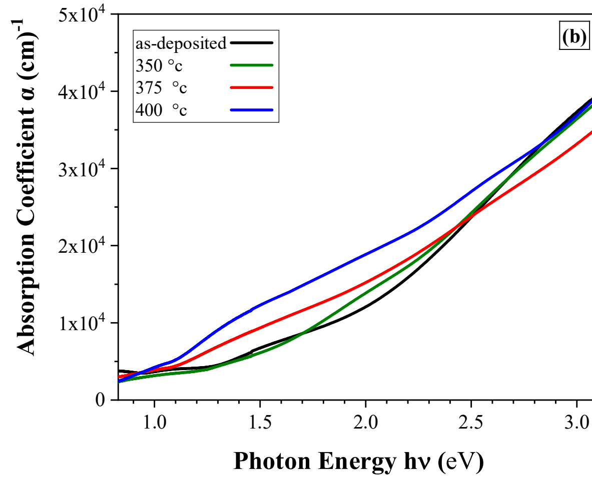

FIG. 4. (a) Transmittance spectra of CZTS thin films, (b) absorption coefficient of CZTS thin.

The thickness of the CZTS films was measured by optical method [28]. It was found to be equal to 1.15 µm for the as-deposited thin film, and equal to 1.13 µm, 1.12 µm, and 1.09 µm, for annealed thin films at 350, 375, and 400 °C, respectively. Thin films show a large value for the absorption coefficient of the order 10^4 cm^{-1} in the visible and near infra-red regions as shown in Fig. 4(b).

The Optical Energy Band Gap E_g for CZTS Thin Films

One of the most important characteristics that determine the applicability of the prepared thin films as a layer in photovoltaic cells is the value of the optical band gap E_g. The value of the optical energy band gap was calculated in the region of intense absorption near the absorption edge using the Tauc's relationship for direct semiconductors as given by the relationship [27]:

$$\alpha h\nu = B(h\nu - E_g)^{1/2} \quad (7)$$

where B is a constant, h is Planck's constant, and ν is the frequency of the incident light beam.

The optical energy gap values of the CZTS thin films were determined by extrapolating the linear part of the $(\alpha h\nu)^2$ vs. $h\nu$ plots to cut off the photon energy axis. Fig. 5 presents $(\alpha h\nu)^2$ vs. $h\nu$ plot of CZTS thin films, the inset shows the variation of E_g as a function of annealing temperature. The obtained E_g values were decreased from 1.66 eV to 1.52 eV. These values are in good agreement with previous studies [29-31].

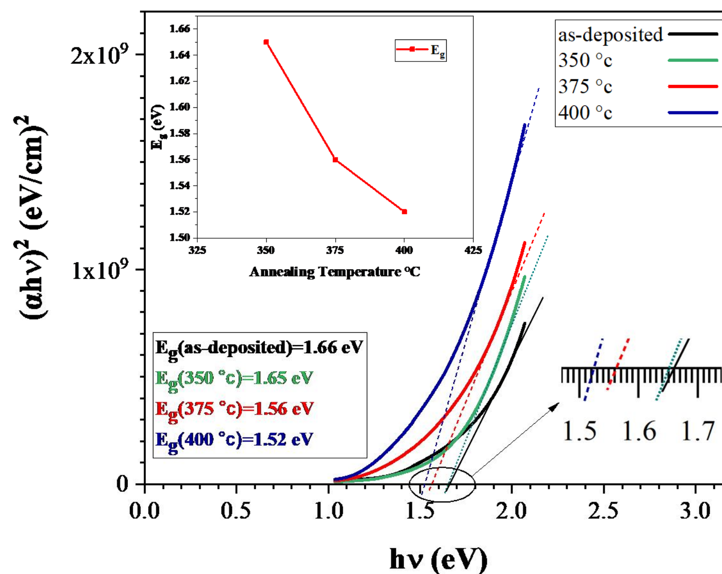

FIG. 5. The dependence of $(\alpha h\nu)^2$ of CZTS thin films versus the photon energy hν, and inset the variation of energy band gap versus annealing temperature.

The grain size enlargement decreases the energy band gap values, as shown in Fig. 3 using AFM images. This was indicated by the decrease in the S_{pd} as a result of the union between the grains forming larger ones. This growth led to a minimization of the quantum confinement effect [32]. The later effects occur for small grain sizes [33], and E_g is red-shifted with growing the size of grains [34].

Absorption Band Tail (Urbach Tail)

The optical absorption spectra of semiconductors play an important role, as they give basic information about their composition. There is an exponential part along the absorption coefficient curve and near the edge of the energy band gap called the Urbach tail. This exponential tail appears in amorphous and weak crystalline materials because these materials have local states that extend to the optical energy band gap [35]. This tail is sometimes called Urbach energy E_U, which is weakly dependent on the temperature and often interpreted as the width of the band tail due to localized states in the energy gap. Such states are usually associated with disordered or low-crystalline materials [36, 37]. Therefore, the E_U can be used as an indicator of the quality of the material. The spectral dependence of the absorption coefficient α on the photon energy $h\nu$ at photon energy less than the E_g is known as Urbach's empirical rule, which is given by the following equation [36]:

$$\alpha = \alpha_0 \exp(E/E_U) \tag{8}$$

where α_0 is constant.

The energy E_U can be determined from the slope of the linear part of ln(α) as a function of the incident photon energy $h\nu$. Table 4 shows the Urbach energy values for CZTS thin films. Fig. 6 shows the ln (α) vs. $h\nu$ of the as-deposited and annealed CZTS films in the tail region. The insets in Fig. (6) illustrate the variation of Urbach energy with annealing temperature. It is noted from Fig. 6 that the Urbach energy decreases with the increase in the annealing temperature. This can be attributed to the improvement of the crystalline structure of the thin films by annealing treatment, which leads to a decrease in the density of localized states, in agreement with the results in Ref. [38]. Our x-ray diffraction study provides evidence for this interpretation. It shows that a pure phase of kesterite was obtained at an annealing temperature of 400 °C.

TABLE 4. Calculated values of optical energy band gap E_g, Urbach energy E_U, refractive index n, and dielectric constants for CZTS films.

Thin Film	Optical band gap E_g (eV)	Urbach energy E_U (eV)	refractive index n	High-frequency dielectric constant ε_∞	dielectric constant ε
As-deposited	1.66	1.32	2.84	8.06	13.41
350 °C	1.65	0.91	2.84	8.09	13.43
375 °C	1.56	0.53	2.88	8.32	13.71
400 °C	1.52	0.39	2.90	8.43	13.83

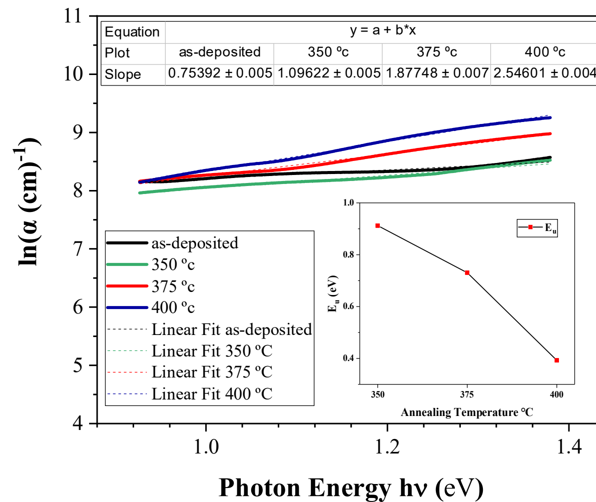

FIG. 6. The dependence of $\ln(\alpha)$ of CZTS thin films versus the photon energy hν, and inset the variation of Urbach energy versus annealing temperature.

Refractive Index n and Dielectric Constants of CZTS Thin Films

The refractive index n of thin films is a key factor for the total internal reflection potential for any photovoltaic cell. The refractive index of CZTS films was calculated using the Moss relation [39]:

$$n = \left(k/E_g\right)^{1/4} \quad (9)$$

where k = 108eV.

The dielectric properties of a material under the influence of an external electric field depend on the degree of its polarization. Materials with suitable dielectric constants are essential to progress efficient photovoltaic cells. The dielectric constant ε of the films was calculated using the relationship [39]:

$$\varepsilon = 18.52 - 3.08E_g \quad (10)$$

The high-frequency dielectric constant ε_∞ of the CZTS thin films was determined using the relationship [39]:

$$\varepsilon_\infty = n^2 \quad (11)$$

Table 4 shows the values of optical energy band gap E_g, Urbach energy E_U, refractive index n, high-frequency dielectric constant ε_∞, and dielectric constant ε of CZTS thin films.

Conclusions

CZTS semiconductor thin films were successfully fabricated on soda-lime glass substrates using a simple and inexpensive sol-gel spin-coating technique. Thin films were annealed in an argon atmosphere at temperatures of 350, 375, 400, 425, and 450 °C for one hour. x-ray diffraction study showed that the as-deposited thin film had a weakly crystalline quaternary kesterite structure. By increasing the annealing temperature up to 400 °C secondary phases of SnS and Cu_2S were eliminated, and a pure phase of kesterite was obtained. However, at even higher temperatures, the kesterite phase had degraded. AFM measurements showed that the surfaces of the films were homogeneous and that the predominant grain growth mode was Volmer–Weber mode. In addition, the surface roughness increased with the escalation of annealing temperatures. CZTS thin films showed a high absorption coefficient of the order of 10^4 cm^{-1}. Additionally, the optical energy band gap (E_g) experienced a redshift, transitioning from 1.66 eV to 1.52 eV with increasing annealing temperature. The Urbach tail study confirmed that the annealing process leads to a decrease in the density of localized states at 400°C annealing temperature, thus getting a pure phase of kesterite. Based on these results, the thin film annealed at 400 °C can be considered a promising absorbent layer for third-generation photovoltaics.

References

[1] Swanson, R.M., Science, 324 (2009) 891.

[2] Su, Z., Sun, K., Han, Z., Liu, F., Lai, Y., Li, J. and Liu, Y., J. Mater. Chem., 22 (2012) 16346.

[3] Akhanda, S., Matin, R., Bashar, M.S., Sultana, M., Kowsar, A., Rahaman, M. and Mahmood, Z.H., Bangladesh J. Sci. Ind. Res., 53 (2018) 13.

[4] Olgar, M.A., Klaer, J., Mainz, R., Ozyuzer, L. and Unold, T., Thin Solid Films, 628 (2017) 1.

[5] Diwate, K., Mohite, K., Shinde, M., Rondiya, S., Pawbake, A., Date, A., Pathan, H. and Jadkar, S., Energy Procedia, 110 (2017) 180.

[6] Liu, C.-Q., Wen, B., Zhai, X.-N., Lun, T.-T., Song, M.-S., Wang, N., Liu, S.-M., Wang, H.-L., Jiang, W.-W., Ding, W.-Y., Xu, S.-C. and Chai, W.-P., Mater. Lett., 213 (2018) 241.

[7] Raiguru, J., Subramanyam, B., Sa, K., Alam, I., Das, S., Mukherjee, J., Mahakul, P.C., Subudhi, B. and Mahanandia, P., IOP Conf. Ser. Mater. Sci. Eng., 178 (2017) 012017.

[8] Pu, A., Ma, F., Yan, C., Huang, J., Sun, K., Green, M. and Hao, X., Sol. Energy Mater. Sol. Cells, 160 (2017) 372.

[9] Kumar, J. and Ingole, S., Mater. Sci. Semicond. Process, 91 (2019) 31.

[10] Ziti, A., Hartiti, B., Labrim, H., Fadili, S., Batan, A., Ridah, A. and Thevenin, P., IOP Conf. Ser. Mater. Sci. Eng., IOP Publishing, (2020) 012025.

[11] Nkuissi Tchognia, J.H., Arba, Y., Dakhsi, K., Hartiti, B., Ndjaka, J.-M., Ridah, A. and Thevenin, P., Opt. Quantum Electron, 48 (2016) 1.

[12] Park, H., Hwang, Y.H. and Bae, B.-S., J. Sol-GelSci. Technol., 65 (2013) 23.

[13] Guo, B.L., Chen, Y.H., Liu, X.J., Liu, W.C. and Li, A.D., AIP Adv., 4 (2014) 097115.

[14] Chalapathi, U., Uthanna, S. and Raja, V.S., Bull. Mater. Sci., 40 (2017) 887.

[15] Park, S.-N., Sung, S.-J., Son, D.-H., Kim, D.-H., Gansukh, M., Cheong, H. and Kang, J.-K., RSC Adv., 4 (2014) 9118.

[16] Sun, L., He, J., Kong, H., Yue, F. and Yang, P., J. Chu, Sol. Energy Mater. Sol. Cells, 95 (2011) 2907.

[17] Kittel, C., Introduction to Solid State Physics, 8th Ed. (John Wiley and Sons, New York, 2005).

[18] Zhang, K.D., Tian, Z.R., Wang, J.B., Li, B., Zhong, X.L., Guo, D.Y. and He, S.M., J. Sol-GelSci. Technol. 73 (2015) 452.

[19] Patterson, A.L., Phys. Rev., 56 (1939) 978.

[20] Williamson, G.K. and Smallman, R.E., Philos. Mag., 1 (1956) 34.

[21] Surgina, G.D., Nevolin, V.N., Sipaylo, I.P., Teterin, P.E., Medvedeva, S.S., Lebedinsky, Y.Y. and Zenkevich, A.V., Thin Solid Films, 594 (2015) 74.

[22] Sharmin, A., Bashar, M.S., Sultana, M. and Al Mamun, S.M.M., AIP Adv., 10 (2020) 015230.

[23] Shahenoor Basha, S.K. and Rao, M.C., Ceram. Int., 1 (2018) 648.

[24] El Kissani, A., Ait el Haj, D., Ait Dads, H., Welatta, F., Nkhaili, L., Assali, K.E. and Outzourhit, A., Spectrosc. Lett., 53 (2020) 123.

[25] Fornari, C.I., Fornari, G., de O. Rappl, P.H. Abramof, E. and J. dos S. Travelho, InTech, (2018) 56552.

[26] Courel, M., Valencia-Resendiz, E., Andrade-Arvizu, J.A., Saucedo, E. and Vigil-Galán, O., Sol. Energy Mater. Sol. Cells, 159 (2017) 151.

[27] Bass, M. (Ed.), "Optical Society of America", (McGraw-Hill, New York, 1995).

[28] Krishnan, A., Rishad Ali, K., Vishnu, G. and Kannan, P., Mater. Renew. Sustain. Energy, 8 (2019) 16.

[29] Liu, R., Tan, M., Zhang, X., Chen, J., Song, S. and Zhang, W., J. Alloys Compd., 655 (2016) 124.

[30] Lu, L., Zheng, T., Wu, Q., Schneider, A.M., Zhao, D. and Yu, L., Chem. Rev., 115 (2015) 12666.

[31] Ziti, A., Hartiti, B., Labrim, H., Fadili, S., Ridah, A., Belhorma, B., Tahri, M. and Thevenin, P., Superlattices Microstruct., 127 (2019) 191.

[32] Neikov, O.D. and Yefimov, N.A., Elsevier, (2008) 634.

[33] Khare, A., Wills, A.W., Ammerman, L.M., Norris, D.J. and Aydil, E.S., Chem. Commun., 47 (2011) 11721.

[34] Kim, C.-D., Kim, H.T., Min, B.-K. and Park, C., Mol. Cryst. Liq. Cryst., 602 (2014) 151.

[35] Melsheimer, J. and Ziegler, D., Thin Solid Films, 129 (1985) 35.

[36] Urbach, F., Phys. Rev., 92 (1953) 1324.

[37] Clark, A.H., "Polycrystalline and amorphous thin films and devices", (Academic Press, New York, 1980).

[38] Larsen, J.K., Scragg, J.J.S., Ross, N. and Platzer-Björkman, C., ACS Appl. Energy Mater., 3 (2020) 7520.

[39] Hannachi, L. and Bouarissa, N., Phys. B Condens. Matter, 404 (2009) 3650.